Desalination and Water Treatment
www.deswater.com

doi: 10.1080/19443994.2015.1058194

57 (2016) 13394–13403
June

Taylor & Francis
Taylor & Francis Group

Photo-corrosion inhibition of Ag_3PO_4 by polyaniline coating

Yunfan Zhang[a], Rengaraj Selvaraj[b,*], Younghun Kim[c], Mika Sillanpää[a,*], Cheuk-Wai Tai[d]

[a]*Laboratory of Green Chemistry, Faculty of Technology, Lappeenranta University of Technology, Mikkeli FI-50100, Finland, email: Mika.Sillanpaa@lut.fi*
[b]*Department of Chemistry, College of Science, Sultan Qaboos University, Muscat, Oman, Tel. +968 2414 2436; email: srengaraj1971@yahoo.com*
[c]*Department of Chemical Engineering, Kwangwoon University, Seoul 139-701, Korea*
[d]*Arrhenius Laboratory, Department of Materials and Environmental Chemistry, Stockholm University, Stockholm S-106 91, Sweden*

Received 8 April 2015; Accepted 30 May 2015

ABSTRACT

In this paper, polyaniline-coated silver phosphate has been successfully prepared via a facile chemisorption method in order to improve the stability of Ag_3PO_4 under light irradiation. The crystalline phase, band gap energy, and microstructure of the obtained PANI/Ag_3PO_4 composites were characterized by X-ray diffraction, UV–vis diffuse reflection spectroscopy, scanning electron microscopy, and transmission electron microscopy, respectively. The photocatalytic degradation of methlylene blue was performed to test the activities of PANI/Ag_3PO_4 composites with different coating amounts and the results indicate that the stabilities of PANI/Ag_3PO_4 composites were successfully enhanced. The correlation between photocatalytic performance and the properties of PANI/Ag_3PO_4 composites is discussed in detail.

Keywords: Polyaniline; Ag_3PO_4; Photocatalyst; Photo-corrosion inhibition; Structural characterization

1. Introduction

Dyes are extensively used for various industrial applications, such as textile, leather tanning, paper and pulp, and food industry, and mainly for coloring [1]. Nowadays, more than 9000 types of dyes have been developed to satisfy numerous industrial demands [2]. In contrast to its functional benefit, color is hazards to the environment due to it being composed of abundant pollutants such as toxic organic residues, acids, bases, and inorganic contaminants [1]. Mutagenic and carcinogenic potentials of azo dye processing plant effluent have been discovered [3]. Therefore, dye removal from industrial effluent is one of the major emergent environmental issues. Many physical and chemical treatment methods, including adsorption [4], coagulation [5], precipitation [6], filtration [7], and oxidation [8], have been developed and applied for color removal. However, physical methods such as activated carbon adsorption are not able to decompose the contaminants and also the used adsorbent is hardly recyclable. By contrast, chemical methods, such as advanced oxidation processes (AOPs), have recently attracted rising attention in the field of effluent treatment, in particular for the removal of

*Corresponding authors.

coloring pollutants [9–11]. Photocatalytic reactions, as AOPs, are able to degrade contaminants by preserving the photocatalyst itself [12]. Photocatalysts are usually solid semiconductors, in which electron–hole pairs are generated by light having the energy higher than the band gap of the material [13]. Desirable properties of an outstanding photocatalyst should be as follows: chemically inert, inexpensive, and non-hazardous as well as possess great photocatalytic activity.

At present, several photocatalysts have been developed to utilize solar spectrum for dye waste degradation. Initially, binary transition metal oxides are noticed as photocatalytic materials. Among those, titanium dioxide (TiO_2) and zinc oxide (ZnO) are most widely used and studied [13]. TiO_2 is a typically n-type semiconductor and its photoelectrochemical property was demonstrated as an anode for water splitting in 1972 [14]. Afterwards, it was used for the remediation of environmental pollutants in 1977 [15]. Zinc oxide has been often considered as a valid alternative to TiO_2 because of its good optoelectronic, catalytic, and photochemical properties. ZnO is active under visible light illumination for the photodegradation of some organic compounds in aqueous solution [13]. Both TiO_2 and ZnO are cheap and non-toxic compounds with strong oxidizing power and have redox selectivity under UV light irradiation, and hence they have been widely studied for environmental purification [16]. Although TiO_2 and ZnO have numerous merits, their shortcomings are also noticeable. First of all, the electron–hole pair generation requires UV light because both TiO_2 and ZnO have wide band gaps. Photocatalysts with wide band gap could limit their application under solar light because the solar spectrum contains only 4% of UV light. On the other hand, zinc oxide is unstable with respect to incongruous dissolution to yield Zn $(OH)_2$ on the particle surface and could further lead to inactivation [17,18]. Therefore, photocatalysts with high performance under visible light irradiation have being developed in the last few decades. Among these photocatalytic semiconductors, CdS [19], Bi_2WO_6 [20], $CaIn_2O_4$ [21], and $CaBi_2O_4$ [22] have been extensively studied. However, their photocatalytic efficiency is still inadequate for industrial application. Recently, it was reported that, as photocatalyst, silver orthophosphate (Ag_3PO_4) exhibits excellent photocatalytic performance in the decomposition of organic contaminants under visible light irradiation [23]. Moreover, the facet effect of Ag_3PO_4 significantly influences its photocatalytic properties [24]. The investigation demonstrates that the crystalline Ag_3PO_4 rhombic dodecahedrons exhibit much higher photocatalytic activities than the cubes for the degradation of organic contaminants. Although Ag_3PO_4 has a good photocatalytic performance, it is easily decomposed when exposed to light. Therefore, the stability of Ag_3PO_4 needs to be enhanced for further applications.

Polyaniline (PANI) as a conducting polymer has been widely studied because of its unique electrical and optical properties as well as excellent environmental stability [25]. Moreover, a number of articles demonstrate that PANI coating could effectively reduce the photo-corrosion of the photocatalyst [26–28]. For example, 1% mass ratio PANI-coated ZnO sample shows no significant decline in the photocatalytic efficiency after recycling thrice [28].

In this paper, monolayer of polyaniline was coated on Ag_3PO_4 surface via a convenient chemisorption approach in order to restrain the photo-corrosion of Ag_3PO_4 under visible light. Photocatalytic experiments exhibit that the photo-corrosion of Ag_3PO_4 was suppressed via polyaniline coating. The possible mechanisms of the inhibition of photo-corrosion have been discussed in detail based on the characterization of obtained samples.

2. Experimental section

2.1. Chemical information

Ammonium phosphate dibasic, silver nitrate, polyaniline, and tetrahydrofuran are all analytical reagents and purchased from Sigma–Aldrich, Finland.

2.2. Synthesis of Ag_3PO_4

Silver phosphate (Ag_3PO_4) samples were firstly synthesized via an ion-exchange method [29]. Initially, 0.003-mol $AgNO_3$ and 0.001-mol $(NH_4)_2HPO_4$ were dissolved into 20-ml and 30-ml deionized water, respectively. Afterwards, $(NH_4)_2HPO_4$ aqueous solution was added dropwise into the prepared $AgNO_3$ solution and was stirred vigorous. The mixed solution was further stirred for another 30 min to ensure sufficient reaction time. Hereafter, the yellow precipitate was separated from the mixed solution by filtration. Finally, the sample was washed with ethanol and distilled water thrice and then dried at 60°C for 10 h.

2.3. Preparation of PANI-coated Ag_3PO_4

PANI/Ag_3PO_4 photocatalysts with different proportions were synthesized as follows [30]: different weights of PANI were dissolved in tetrahydrofuran (THF) to obtain solutions with concentration of 0.2, 0.4, 0.5, and 0.6 g/L, respectively, and then appropriate amounts of Ag_3PO_4 were added into 50-ml PANI/THF solution, sonicated for 30 min, and stirred for 24 h. PANI/Ag_3PO_4 samples were separated from the

solution, washed thrice with water and ethanol, and eventually dried at 80˚C for 24 h. Following this procedure, PANI/Ag_3PO_4 composites with mass ratios 1.0, 2.0, 2.5, and 3.0% were fabricated and labeled, respectively, as PANI/Ag_3PO_4-1, PANI/Ag_3PO_4-2, PANI/Ag_3PO_4-2.5, and PANI/Ag_3PO_4-3.

2.4. Sample characterization

The crystal structure of the prepared samples was identified by an X-ray diffractometer. The graphite monochromatic radiation Cu–Kα1 with wavelength 1.5406 Å was used as the source; the accelerating voltage and the emission current were 40 kV and 100 mA, respectively. For each sample, the scanning range 2θ is from 10˚ to 80˚ and the scanning speed is 0.02˚ per second.

The morphology and microstructure were characterized by cold field emission scanning electron microscopy (FE-SEM, Hitachi S-4800), which was equipped with an energy-dispersive X-ray spectrometer (EDAX Genesis 2). Qualitative and quantitative analyses of the chemical composition of samples were also carried out. The operating voltage was 30 kV and the emission current was 20 nA. The backscattered electrons were used for forming images. Transmission electron microscopy was carried out in a 200-kV Schotty field emission microscope (JEOL JEM-2100F). In order to minimize artifacts during sample preparation, TEM samples were prepared by crushing and the powders were deposited on Cu-supporting grids with holey carbon-supporting films.

In order to determine the chemical states of the samples, X-ray photoelectron spectroscopy (XPS) was performed using a Sigma Probe (Thermo VG, UK) X-ray photoelectron spectrometer. Al–Kα radiation (1.486 eV) was used during the measurement. Photoemitted electrons from the surface of samples were analyzed in a hemispherical energy analyzer at a pass energy of $E_p = 20$ eV. For a survey spectrum, the scanned energy range was from 0.00 to 1,000.00 in 1.00 eV steps. In the slow scanning mode, all spectra were obtained with an energy step of 0.1 eV and a dwell time of 50 ms. Data analysis was performed by a software package from Avantage Thermo VG.

UV–vis diffuse reflectance spectra of the samples were recorded in the wavelength range between 200 and 1,000 nm using a spectrophotometer (V-670, JASCO), with $BaSO_4$ as a reference.

2.5. Photocatalytic reactivity examination

Photocatalytic properties of PANI/Ag_3PO_4 were evaluated by degradation of methylene blue (MB) under a 150-W sodium lamp irradiation. For each experiment, 100-mg PANI/Ag_3PO_4 was initially mixed with 100-ml MB solution (5 ppm) in a Pyrex glass reactor with a cooling water jacket. Then, the mixed solution was sonicated for 5 min to disperse the mixture into suspension. The suspended solution was magnetically stirred in dark for 30 min to reach adsorption/desorption equilibrium. Under the sodium lamp irradiation, the suspension was constantly stirred; and at certain time intervals, aqueous samples were taken and centrifuged to separate photocatalysts from the suspension solution. The reaction temperature was maintained at ~20˚C and an air pump was used to induce air to the system throughout the entire experiment. Separated aquatic samples, eventually, were further analyzed by the Lambda 45 UV–vis spectrometer (PerkinElmer) to determine concentrations of the MB solution at different time intervals. The scanning range was from 800 to 200 nm. The residual concentration of MB solutions was calculated by utilizing the absorbance of MB at 664 nm based on the following equation:

$$\frac{C_t}{C_0} = \frac{A_t}{A_0} \tag{1}$$

C_0 and C_t are the initial concentrations of MB and that of at time t. A_0 and A_t represent the measured absorbance of MB at 664 nm at initial time and after t time reaction, respectively.

3. Results and discussion

3.1. Structural analysis

X-ray diffraction (XRD) patterns of PANI/Ag_3PO_4 with different compositions are shown in Fig. 1. All patterns were well indexed with JCPD (06-0505) standard, with primary diffraction peaks at 20.84˚, 29.64˚, 33.26˚, 36.54˚, 52.66˚, 55.0˚, and 57.24˚ which perfectly matched (1 1 0), (2 0 0), (2 1 0), (2 1 1), (2 2 2), (3 2 0), and (3 2 1) crystallographic planes, respectively. It indicates that all samples were identified as body-centered cubes Ag_3PO_4 with the lattice parameter of 6.006 Å. However, no peaks assigned to PANI were observed because of the low amount of PANI. There were no obvious changes on XRD patterns after PANI was loaded, which confirms that PANI did not cause any structural changes in Ag_3PO_4.

3.2. Photocatalysis performance

Visible light-driven photocatalytic degradation reactions of MB with different PANI/Ag_3PO_4 were

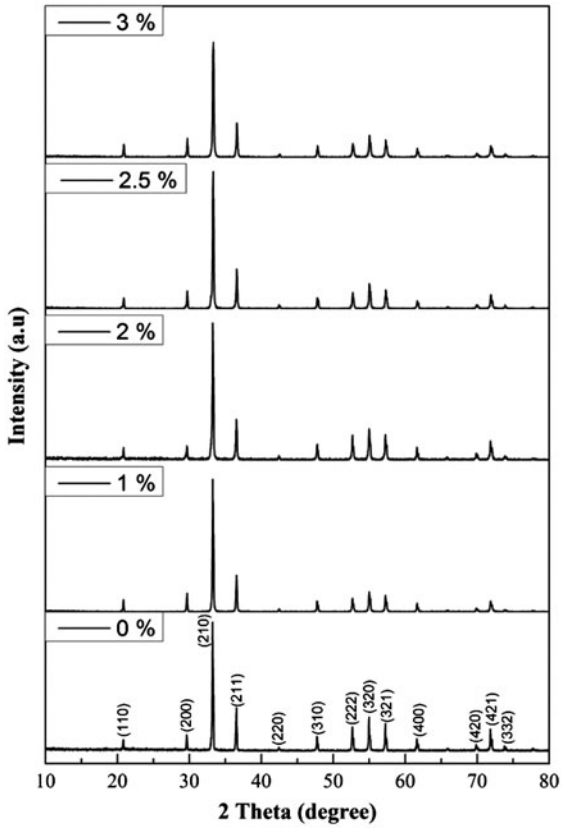

Fig. 1. XRD patterns of Ag_3PO_4 and PANI/Ag_3PO_4 with different mass ratios.

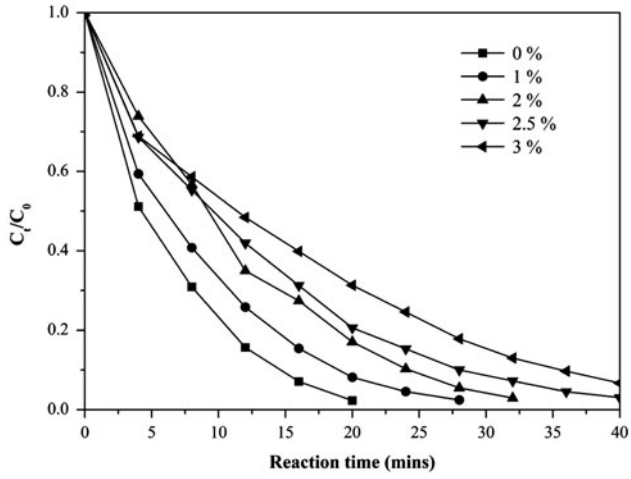

Fig. 2. Plots of degradation rate and reaction time with different PANI/Ag_3PO_4 photocatalysts.

carried out. Two-ml aqueous samples were taken every 4 min for determining the concentration of MB in the solution by UV–vis spectroscopy. The relationship between the degradation rate and reaction time is shown in Fig. 2. It is clear that pure Ag_3PO_4 had the best performance of photocatalytic degradation of the MB solution and the degradation ratio was more than 97% after 20 min of the reaction under visible light irradiation. Moreover, the loading amount of PANI apparently influences the photocatalyic activity. The reaction time for a complete degradation was prolonged with increasing the coating amount of PANI. When the amount of PANI is 3%, only the degradation ratio was 93% after 40 min of light irradiation. The possible explanation is that light penetration is obstructed by the polyaniline molecular structure, and hence the photocatalytic performance of Ag_3PO_4 reduces.

The recycling test of Ag_3PO_4 and PANI/Ag_3PO_4-1 was also conducted in order to investigate their reactive stabilities in photocatalytic degradation of MB. After each photocatalytic experiment, photocatalysts were recycled, washed with deionized water and ethanol for thrice, and subsequently dried at 80˚C for 10 h. Degradation ratios of each experiment vs. reaction time are illustrated in Fig. 3. For the Ag_3PO_4 photocatalyst, its photocatalytic efficiency rapidly reduced to 80% after the first cycle and progressively decreased with recycling frequency or reaction times. In the fifth run, it took 40 min to degrade MB solution completely. In other words, the efficiency of Ag_3PO_4 had been halved after recycling it for four times. By contrast, the photo-stability of PANI/Ag_3PO_4-1 is significantly enhanced when compared to the Ag_3PO_4, though a reduced reaction rate was observed. It is found that the photocatalytic efficiency of PANI/Ag_3PO_4-1 was still as high as 88.8%, even after being recycled for four times. This finding indicates clearly that the photo-corrosion of Ag_3PO_4 was inhibited under the PANI layer protection. It is evident that the polyaniline layer promotes photo-stability of Ag_3PO_4 under visible light. It is also worth noticing that the PANI/Ag_3PO_4 photocatalyst was more efficient at the fifth run when compared with pure Ag_3PO_4.

3.3. Diffuse reflection spectroscopy analysis

UV–vis diffuse reflectance spectra of samples are shown in Fig. 4. It is noticeable that Ag_3PO_4 absorbs light with the wavelength shorter than 530 nm, and therefore the band gap of Ag_3PO_4 could be deduced as 2.34 eV, which is well agreed with previous works [23,31]. Furthermore, the absorption of PANI/Ag_3PO_4 is stronger than that of pure Ag_3PO_4. The absorption edge of the PANI-coated samples was shifted toward higher wavelengths. The high absorption of PANI/Ag_3PO_4 in the visible region is attributed to excellent

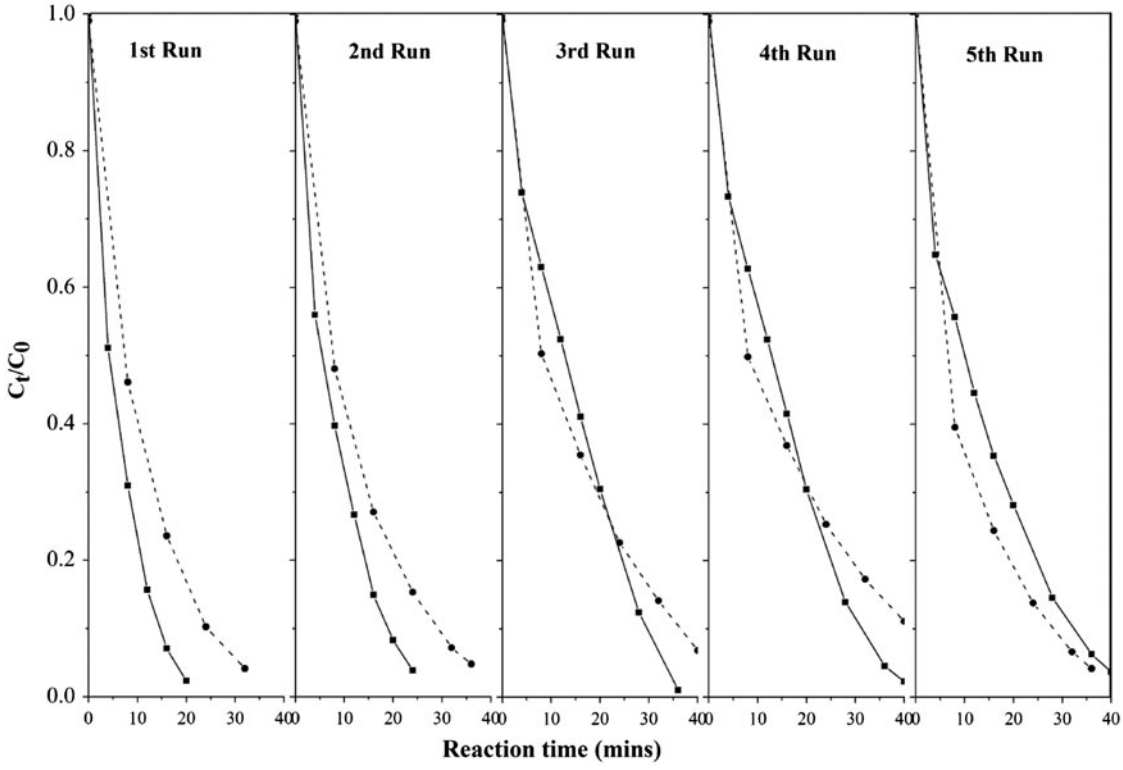

Fig. 3. Cycling photodegradation performance of MB in the presence of Ag_3PO_4 (solid line with cube symbol) and PANI/Ag_3PO_4-1 (dash line with dot symbol).

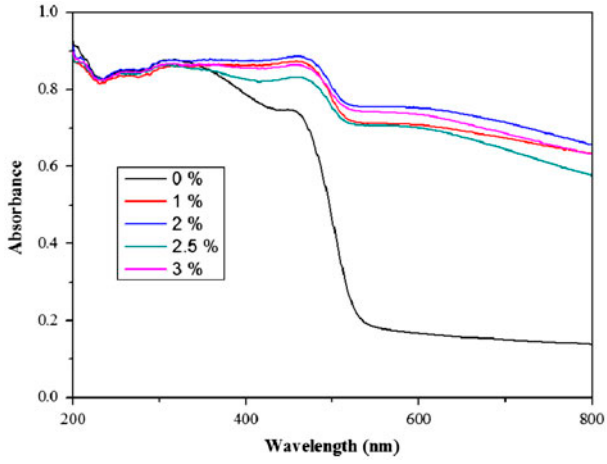

Fig. 4. UV–vis diffuse reflectance spectra of PANI/Ag_3PO_4 with different PANI contents.

photoelectric properties of polyaniline. The conducting polymer, polyaniline, composed of benzenoid and quinonoid units with a delocalized conjugated structure has several redox states [32]. The synergic effect drives the transfer of the excited-state electron from PANI to the conduction band of Ag_3PO_4. This results in the shift of the absorption edge of silver Ag_3PO_4. Similar phenomena have also been reported in previous studies [33,34].

3.4. SEM and EDS analyses

The morphology of the as-prepared photocatalysts was inspected by scanning electron microscopy (SEM). It can be clearly seen in Fig. 5(A) that the Ag_3PO_4 sample exhibited irregular spherical-like morphology and non-uniform diameters. Such results are similar to the previous work [31]. However, the coated PANI layer was not observed from SEM images because PANI molecules were dispersed on the surface of the photocatalyst with a monolayer structure, with a thickness of 0.7–0.8 nm [30], and therefore, it was too thin to be detected by SEM. Furthermore, comparing PANI-coated samples with un-coated samples, pure Ag_3PO_4 particles possess smooth surface and PANI/Ag_3PO_4-1 has a coarse surface.

Elemental analysis of selected samples was performed by EDS, and the typical spectra of samples are shown in Fig. S1. The analysis confirmed that only silver, phosphorous, oxygen, and carbon exist in the samples and all the observed peaks are ascribed on

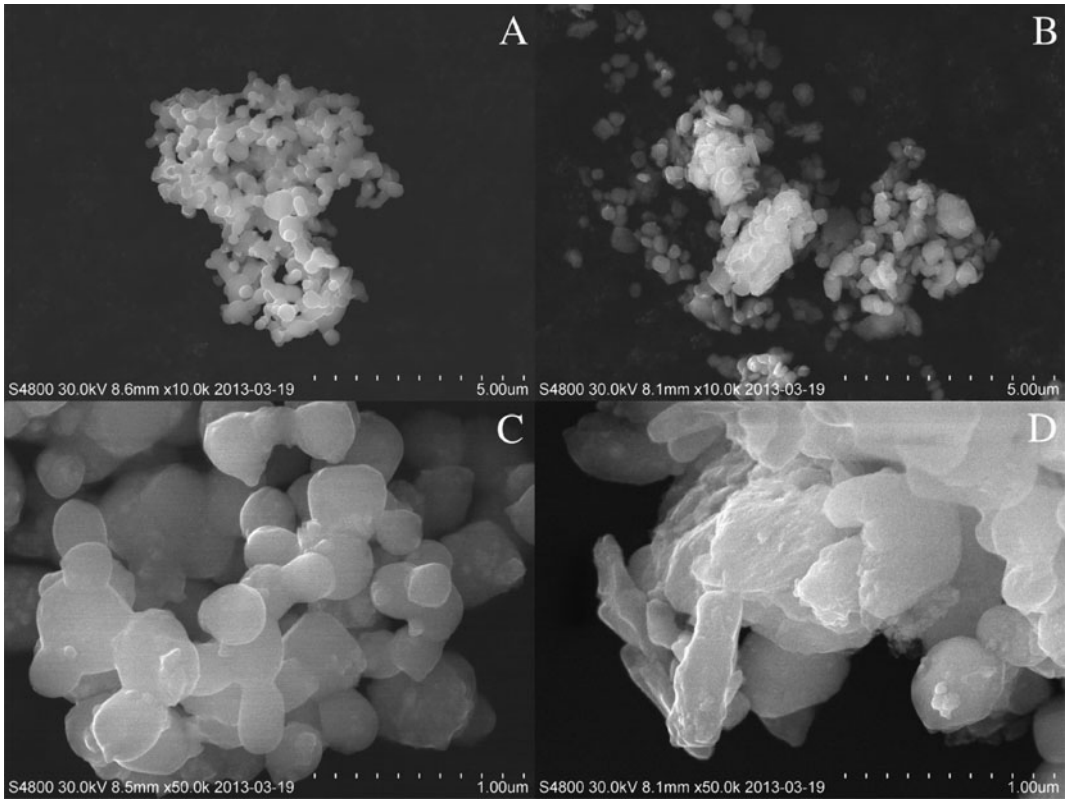

Fig. 5. SEM images of the as-prepared photocatalysts: (A and C) Ag_3PO_4; (B and D): PANI/Ag_3PO_4-1.

the spectrum. Among all the peaks, the three strong peaks observed at 2.98, 3.15, and 3.35 keV correspond to the silver L_α, $L_{\beta1}$, and $L_{\beta2}$ lines. The peaks at 2.01 and 0.52 keV were attributed to phosphorous and oxygen, respectively. Small amounts of carbon, which came from the carbon conductive tapes and coated polyaniline, were detected. The semi-quantitative elemental analysis of Ag_3PO_4 and PANI–Ag_3PO_4-1 was also performed. The atomic ratio of Ag, P, and O in samples was calculated and listed in the corresponding spectrum, respectively. It should be noted that the small difference between measured and theoretical atomic ratio may be caused by various factors, including the thickness variation, particle size, the existence of pores or defects, Cliff–Lorimer factors used, etc. Distributions of silver, phosphorus, and oxygen in pure Ag_3PO_4 and PANI/Ag_3PO_4-1were illustrated by elemental mappings, displayed in Fig. S2. The mapping confirmed the homogeneous distribution of Ag, P, and O in Ag_3PO_4 particles.

3.5. XPS characterization

The XPS was conducted in order to study the composition of prepared samples. The survey spectrum of PANI/Ag_3PO_4-1 only contains the peaks of silver, oxygen, phosphorus, and carbon, indicating no trace of impurity. XPS spectra for Ag 3d, P 2p, and O 1s were acquired in the slow scanning mode, and are shown in Fig. 6. The existence of carbon peak was mainly attributed to polyaniline. In the spectrum, the first peak at 284.8 eV was attributed to C atoms bound only to C or H atoms. In Fig. 6(A), a peak at 288.2 eV shifting from 287.8 eV indicated the links between C and O to form O–C=N structure. The spectrum of O 1s (Fig. 6(B)) contains two peaks at 530.5 and 532.2 eV, which are derived from P–O and P=O bonding, respectively [35,36]. After PANI was coated on Ag_3PO_4, two oxygen peaks were shifted to 530.7 and 532.4, respectively. Such peak shifts indicate the bonding between O and C. Ag 3d spectra of silver phosphate (Fig. 6(C)) were composed of two strong peaks at 367.8 and 373.8 eV, which were assigned to Ag $3d_{3/2}$ and Ag $3d_{5/2}$ binding energies, respectively [37]. These two Ag 3d peaks were ascribed to the Ag^+ of Ag_3PO_4 [38,39]. P 2p spectra (Fig. 6(D)) of Ag_3PO_4 contain a peak at 132.5 eV that related to phosphorous ion (P^{5+}) [40]. When PANI was loaded on the surface of Ag_3PO_4, the binding energy of P 2p shifted from 132.5 to 132.7 eV. This result suggests that the

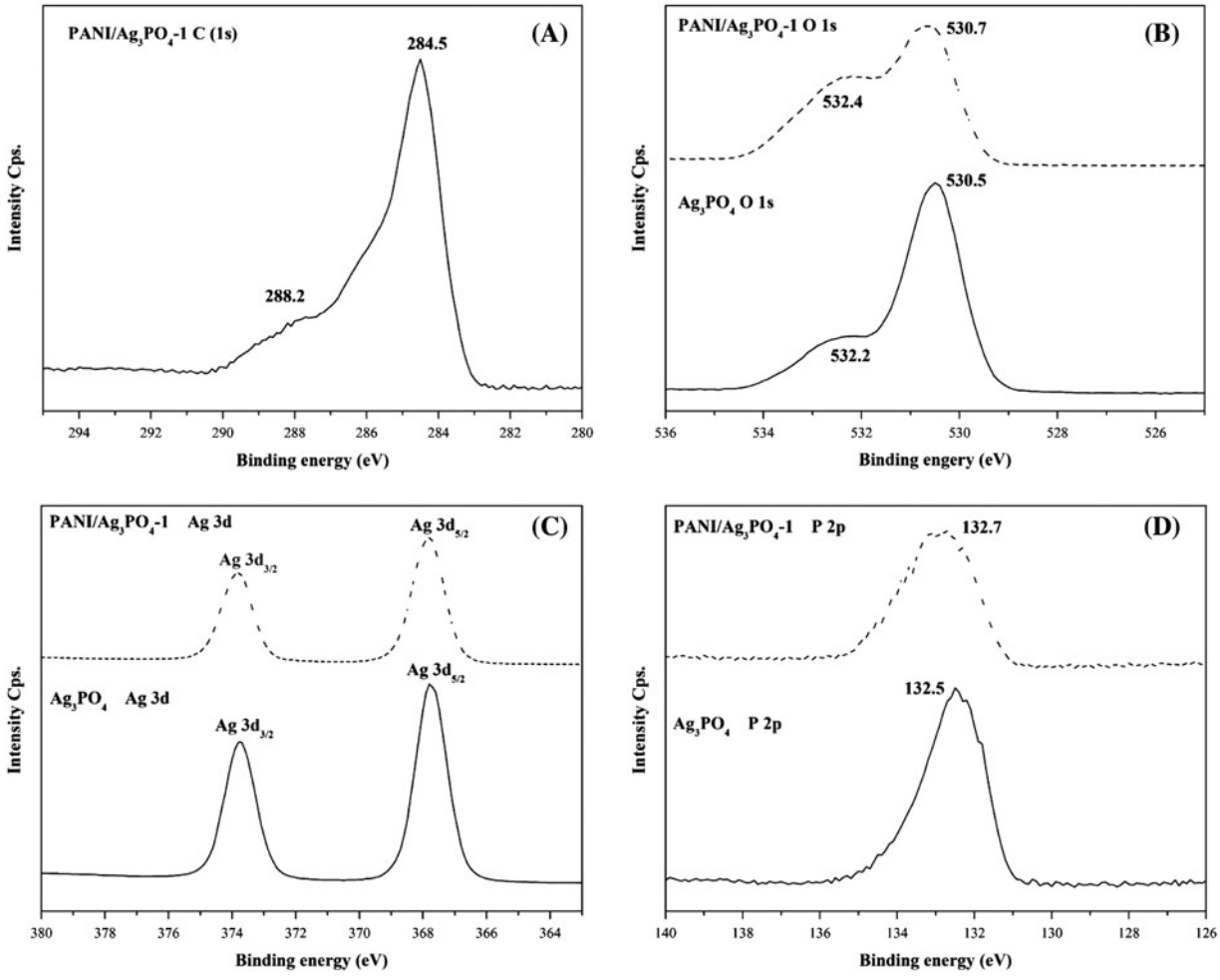

Fig. 6. XPS spectra of the PANI/Ag_3PO_4-1: (A) scanning spectrum, (B) Ag 3d, (C) O 1s, and (D) P 2p.

structure of O–C=N–P constitutes a stronger binding force due to the interaction between Ag_3PO_4 and polymer.

3.6. Mechanism discussion

Ag_3PO_4 can be readily decomposed under visible light in the process of water oxidation, which can be expressed in following chemical formula [23]:

$$Ag_3PO_4 + 6H_2O + 12h^+ + 12e^- \rightarrow 12Ag + 4H_3PO_4 + 3O_2$$

It can be noted easily that both photo-generated electrons and holes are required to achieve the photo-decomposition of Ag_3PO_4. In other words, if photo-generated electrons and holes could be separated from the chemical reaction above, the photo-decomposition of Ag_3PO_4 may be retarded or prevented. The mechanism of photocatalytic degradation of MB in Ag_3PO_4 system has also been shown by the reactive oxygen species trapping experiments [29]. The results indicated that the reactive species generated from photo-generated holes are mainly involved in the degradation of MB over Ag_3PO_4.

Typical bright-field TEM images of Ag_3PO_4 with and without PANI are shown in Fig. 7. It can be seen clearly that a single Ag_3PO_4 particle was coated by PANI layer with the thickness of about 4–5 nm. As a conducting polymer, PANI composed of benzenoid and quinonoid units with delocalized conjugated structures has several redox states. The combination of Ag_3PO_4 and PANI with conjugated structure is matched well at the energy level [23,41], which has been shown by the shift of absorption edge of

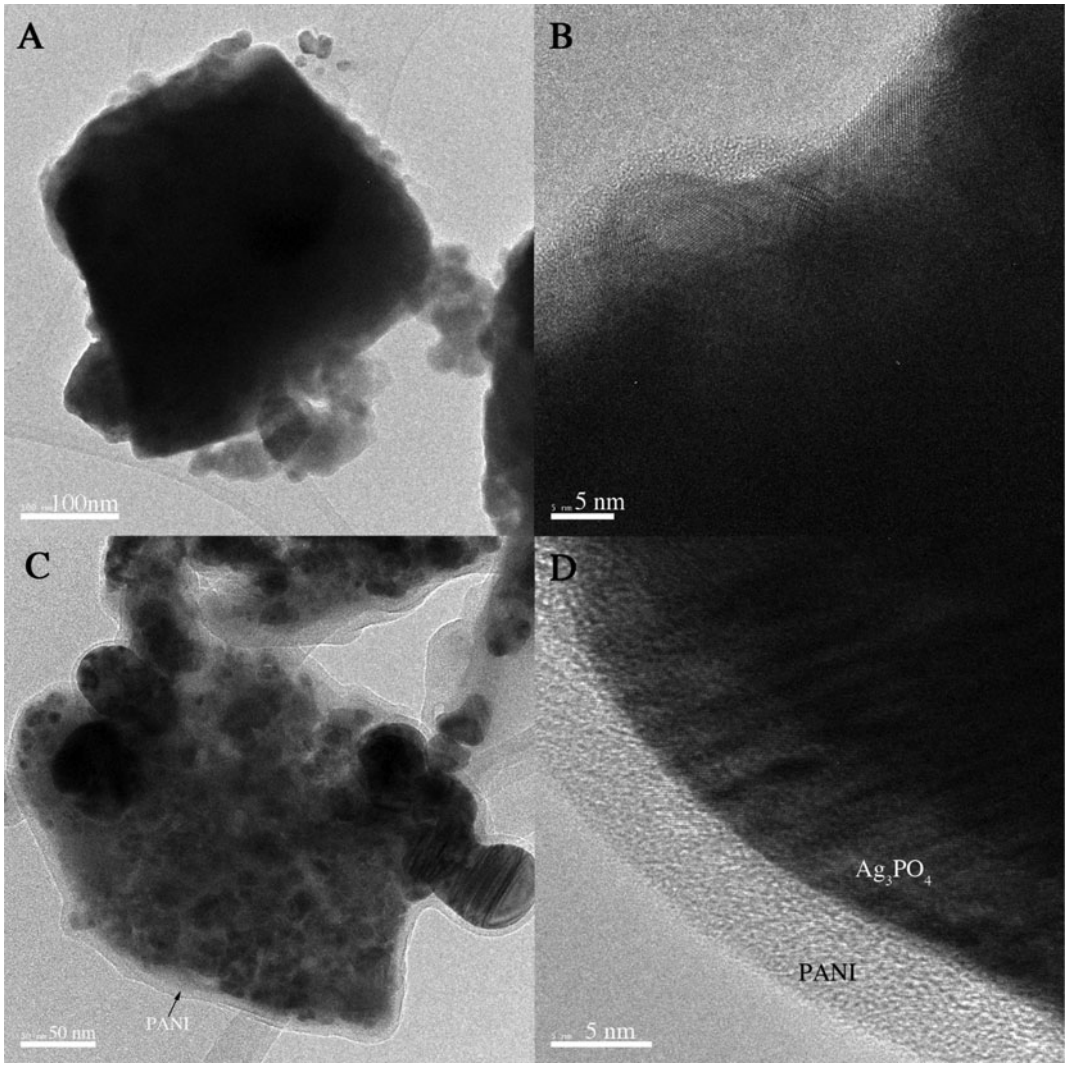

Fig. 7. TEM images of Ag_3PO_4 (A and B) and PANI/Ag_3PO_4 (C and D) at different magnifications.

PANI–Ag_3PO_4 on UV–vis diffuse reflectance spectrum. As the result, PANI/Ag_3PO_4 was a good system to separate photo-generated charge carriers.

The mechanism of the charge separation and photocatalysis over PANI–Ag_3PO_4 photocatalyst is depicted in Fig. 8. Ag_3PO_4 possesses a lower conduction band position (0.45 eV) [23] than the lowest unoccupied molecular orbital of PANI (−2.10 eV) [42]; so, the hybrid photocatalyst photo-generated electrons, preferably transfer to the former. Moreover, the valence band position of Ag_3PO_4 (2.90) [23] is lower than the highest occupied molecular orbital (HOMO) of PANI (0.70) [42]. Therefore, the hybrid photocatalyst photo-generated holes tend to move to the latter. When PANI–Ag_3PO_4 composite material is under visible light irradiation, both PANI and Ag_3PO_4 are excited, and hence generate the charge carriers. The excited electrons in PANI can easily transfer to the conduction band in Ag_3PO_4. Simultaneously, the photo-generated holes in valence band of Ag_3PO_4 can easily move to the HOMO of PANI. As the result, the photo-generated holes transfer onto the PANI surface, whereas the photo-generated electrons are transported to Ag_3PO_4 surface. Consequently, the holes can combine with hydroxide ions to form highly reactive hydroxyl radicals and the accumulated electrons on the Ag_3PO_4 surface can react with O_2 to yield $\cdot O_2^-$ ($O_2/\cdot O_2^-$, 0.48 V vs. Ag/AgCl). Thus, the decomposition of Ag_3PO_4 by light is significantly reduced because electrons and holes were consumed in the production of hydroxyl radicals and $\cdot O_2^-$, respectively.

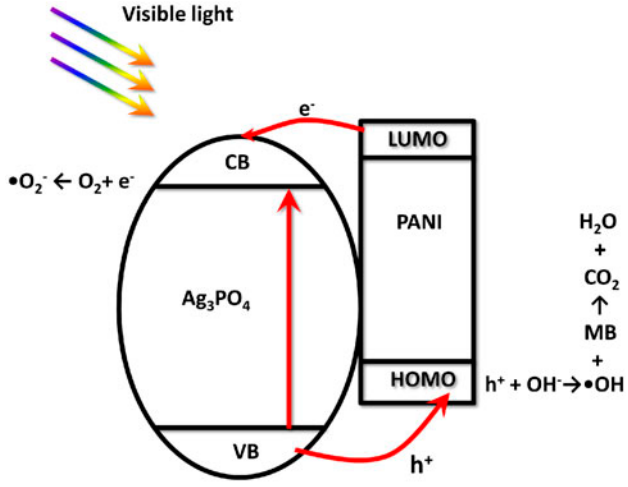

Fig. 8. The schematic diagram of visible light photocatalysis on the PANI/Ag_3PO_4 system.

4. Conclusions

In this work, it demonstrated that the photo-stability of silver orthophosphate has been enhanced by coating polyaniline via a chemisorption approach. The relationship between the coating amount and photocatalytic performance has been studied and the results show that the polyaniline coating could effectively inhibit the decomposition of Ag_3PO_4 and also decrease the efficiency. The improved stability of PANI/Ag_3PO_4 composite is attributed to remarkable delocalized conjugated structure of polyaniline and its effect on charge separation in the composite. Thus, it could be concluded that polyaniline coating could be an efficient way to prevent the decomposition of Ag_3PO_4 during photocatalytic reaction.

Acknowledgments

The authors would like to acknowledge the support provided by MVTT Foundation. The Knut and Alice Wallenberg Foundation is acknowledged for an equipment grant for the electron microscopy facilities in Stockholm University and financial support to C.W.T. under the project 3DEM-NATUR.

Supplementary data

The supplementary material for this paper is available online at http://dx.doi.10.1080/19443994.2015.1058194.

References

[1] M. Hasnain Isa, L. Siew Lang, F.A.H. Asaari, H.A. Aziz, N. Azam Ramli, J.P.A. Dhas, Low cost removal of disperse dyes from aqueous solution using palm ash, Dyes Pigm. 74 (2007) 446–453.
[2] V. Garg, R. Gupta, A. Bala Yadav, R. Kumar, Dye removal from aqueous solution by adsorption on treated sawdust, Bioresour. Technol. 89 (2003) 121–124.
[3] R.O. Alves de Lima, A.P. Bazo, D.M.F. Salvadori, C.M. Rech, D. de Palma Oliveira, G. de Aragão Umbuzeiro, Mutagenic and carcinogenic potential of a textile azo dye processing plant effluent that impacts a drinking water source, Mutat. Res. Genet. Toxicol. Environ. Mutagen. 626 (2007) 53–60.
[4] M.M. Ayad, A.A. Abu El-Nasr, J. Stejskal, Kinetics and isotherm studies of methylene blue adsorption onto polyaniline nanotubes base/silica composite, J. Ind. Eng. Chem. 18 (2012) 1964–1969.
[5] M.A. Hasnat, J.A. Safwan, M.S. Islam, Z. Rahman, M.R. Karim, T.J. Pirzada, A.J. Samed, M.M. Rahman, Electrochemical decolorization of Methylene blue at Pt electrode in KCl solution for environmental remediation, J. Ind. Eng. Chem. 21 (2015) 787–791.
[6] Y.-C. Lee, E.J. Kim, J.-W. Yang, H.-J. Shin, Removal of malachite green by adsorption and precipitation using aminopropyl functionalized magnesium phyllosilicate, J. Hazard. Mater. 192 (2011) 62–70.
[7] A. Tawfik, D.F. Zaki, M.K. Zahran, Degradation of reactive dyes wastewater supplemented with cationic polymer (Organo Pol.) in a down flow hanging sponge (DHS) system, J. Ind. Eng. Chem. 20 (2014) 2059–2065.
[8] L. Yue, K. Wang, J. Guo, J. Yang, X. Luo, J. Lian, L. Wang, Enhanced electrochemical oxidation of dye wastewater with Fe_2O_3 supported catalyst, J. Ind. Eng. Chem. 20 (2014) 725–731.
[9] I.K. Konstantinou, T.A. Albanis, TiO_2-assisted photocatalytic degradation of azo dyes in aqueous solution: Kinetic and mechanistic investigations, Appl. Catal., B 49 (2004) 1–14.
[10] S. Vilhunen, M. Sillanpää, Recent developments in photochemical and chemical AOPs in water treatment: A mini-review, Rev. Environ. Sci. Biotechnol. 9 (2010) 323–330.
[11] M. Karatas, Y.A. Argun, M.E. Argun, Decolorization of antraquinonic dye, reactive blue 114 from synthetic wastewater by Fenton process: Kinetics and thermodynamics, J. Ind. Eng. Chem. 18 (2012) 1058–1062.
[12] M.N. Chong, B. Jin, C.W. Chow, C. Saint, Recent developments in photocatalytic water treatment technology: A review, Water. Res. 44 (2010) 2997–3027.
[13] A. Di Paola, E. García-López, G. Marcì, L. Palmisano, A survey of photocatalytic materials for environmental remediation, J. Hazard. Mater. 211–212 (2012) 3–29.
[14] A. Fujishima, K. Honda, Electrochemical photolysis of water at a semiconductor electrode, Nature 238 (1972) 37–38.
[15] S.N. Frank, A.J. Bard, Heterogeneous photocatalytic oxidation of cyanide ion in aqueous solutions at titanium dioxide powder, J. Am. Chem. Soc. 99 (1977) 303–304.
[16] A. Fujishima, T.N. Rao, D.A. Tryk, Titanium dioxide photocatalysis, J. Photochem. Photobiol., C 1 (2000) 1–21.
[17] A.J. Hoffman, E.R. Carraway, M.R. Hoffmann, Photocatalytic production of H_2O_2 and organic peroxides on quantum-sized semiconductor colloids, Environ. Sci. Technol. 28 (1994) 776–785.

[18] D.W. Bahnemann, C. Kormann, M.R. Hoffmann, Preparation and characterization of quantum size zinc oxide: A detailed spectroscopic study, J. Phys. Chem. 91 (1987) 3789–3798.
[19] N. Kakuta, K. Park, M. Finlayson, A. Ueno, A. Bard, A. Campion, M. Fox, S. Webber, J. White, Photoassisted hydrogen production using visible light and coprecipitated zinc sulfide.cntdot.cadmium sulfide without a noble metal, J. Phys. Chem. 89 (1985) 732–734.
[20] L. Zhang, H. Wang, Z. Chen, P.K. Wong, J. Liu, Bi_2WO_6 micro/nano-structures: Synthesis, modifications and visible-light-driven photocatalytic applications, Appl. Catal., B 106 (2011) 1–13.
[21] J. Tang, Z. Zou, J. Yin, J. Ye, Photocatalytic degradation of methylene blue on $CaIn_2O_4$ under visible light irradiation, Chem. Phys. Lett. 382 (2003) 175–179.
[22] J. Tang, Z. Zou, J. Ye, Efficient photocatalytic decomposition of organic contaminants over $CaBi_2O_4$ under visible-light irradiation, Angew. Chem. Int. Ed. 43 (2004) 4463–4466.
[23] Z. Yi, J. Ye, N. Kikugawa, T. Kako, S. Ouyang, H. Stuart-Williams, H. Yang, J. Cao, W. Luo, Z. Li, An orthophosphate semiconductor with photooxidation properties under visible-light irradiation, Nat. Mater. 9 (2010) 559–564.
[24] Y. Bi, S. Ouyang, N. Umezawa, J. Cao, J. Ye, Facet effect of single-crystalline Ag_3PO_4 sub-microcrystals on photocatalytic properties, J. Am. Chem. Soc. 133 (2011) 6490–6492.
[25] X. Li, D. Wang, G. Cheng, Q. Luo, J. An, Y. Wang, Preparation of polyaniline-modified TiO_2 nanoparticles and their photocatalytic activity under visible light illumination, Appl. Catal., B 81 (2008) 267–273.
[26] H. Zhang, Y. Zhu, Significant visible photoactivity and antiphotocorrosion performance of CdS photocatalysts after monolayer polyaniline hybridization, J. Phys. Chem. C 114 (2010) 5822–5826.
[27] S. Zhang, Q. Chen, D. Jing, Y. Wang, L. Guo, Visible photoactivity and antiphotocorrosion performance of PdS–CdS photocatalysts modified by polyaniline, Int. J. Hydrogen Energy 37 (2011) 791–796.
[28] H. Zhang, R. Zong, Y. Zhu, Photocorrosion inhibition and photoactivity enhancement for zinc oxide via hybridization with monolayer polyaniline, J. Phys. Chem. C 113 (2009) 4605–4611.
[29] M. Ge, N. Zhu, Y. Zhao, J. Li, L. Liu, Sunlight-assisted degradation of dye pollutants in Ag_3PO_4 suspension, Ind. Eng. Chem. Res. 51 (2012) 5167–5173.
[30] H. Zhang, R. Zong, J. Zhao, Y. Zhu, Dramatic visible photocatalytic degradation performances due to synergetic effect of TiO_2 with PANI, Environ. Sci. Technol. 42 (2008) 3803–3807.
[31] Y. Liu, L. Fang, H. Lu, L. Liu, H. Wang, C. Hu, Highly efficient and stable Ag/Ag_3PO_4 plasmonic photocatalyst in visible light, Catal. Commun. 17 (2012) 200–204.
[32] E. Kang, K. Neoh, K. Tan, Polyaniline: A polymer with many interesting intrinsic redox states, Prog. Polym. Sci. 23 (1998) 277–324.
[33] C. Leng, J. Wei, Z. Liu, R. Xiong, C. Pan, J. Shi, Facile synthesis of PANI-modified $CoFe_2O_4$–TiO_2 hierarchical flower-like nanoarchitectures with high photocatalytic activity, J. Nanopart. Res. 15 (2013) 1–11.
[34] P. Xiong, Q. Chen, M. He, X. Sun, X. Wang, Cobalt ferrite-polyaniline heteroarchitecture: A magnetically recyclable photocatalyst with highly enhanced performances, J. Mater. Chem. 22 (2012) 17485–17493.
[35] S. Tosatti, R. Michel, M. Textor, N. Spencer, Self-assembled monolayers of dodecyl and hydroxy-dodecyl phosphates on both smooth and rough titanium and titanium oxide surfaces, Langmuir 18 (2002) 3537–3548.
[36] Q. Wang, H. Yu, L. Zhong, J. Liu, J. Sun, J. Shen, Incorporation of silver ions into ultrathin titanium phosphate films: In situ reduction to prepare silver nanoparticles and their antibacterial activity, Chem. Mater. 18 (2006) 1988–1994.
[37] H. Zhang, G. Wang, D. Chen, X. Lv, J. Li, Tuning photoelectrochemical performances of Ag−TiO_2 nanocomposites via reduction/oxidation of Ag, Chem. Mater. 20 (2008) 6543–6549.
[38] P. Wang, B. Huang, X. Qin, X. Zhang, Y. Dai, M.-H. Whangbo, $Ag/AgBr/WO_3H_2O$: Visible-light photocatalyst for bacteria destruction, Inorg. Chem. 48 (2009) 10697–10702.
[39] M.S.A.S. Shah, M. Nag, T. Kalagara, S. Singh, S.V. Manorama, Silver on PEG-PU-TiO_2 polymer nanocomposite films: An excellent SYSTEM for antibacterial applications, Chem. Mater. 20 (2008) 2455–2460.
[40] R. Zheng, L. Lin, J. Xie, Y. Zhu, Y. Xie, State of doped phosphorus and its influence on the physicochemical and photocatalytic properties of P-doped titania, J. Phys. Chem. C 112 (2008) 15502–15509.
[41] G. Senadeera, T. Kitamura, Y. Wada, S. Yanagida, Deposition of polyaniline via molecular self-assembly on TiO_2 and its uses as a sensitiser in solid-state solar cells, J. Photochem. Photobiol., A 164 (2004) 61–66.
[42] W. Wu, S. Liang, L. Shen, Z. Ding, H. Zheng, W. Su, L. Wu, Preparation, characterization and enhanced visible light photocatalytic activities of polyaniline/Bi_3NbO_7 nanocomposites, J. Alloys Compd. 520 (2012) 213–219.